

# Disorder-induced half-integer quantized conductance plateau in quantum anomalous Hall insulator–superconductor structures

Yingyi Huang,<sup>1,2</sup> F. Setiawan,<sup>1</sup> and Jay D. Sau<sup>1</sup>

<sup>1</sup>*Department of Physics, Condensed Matter Theory Center and Joint Quantum Institute, University of Maryland, College Park, Maryland 20742, USA*

<sup>2</sup>*State Key Laboratory of Optoelectronic Materials and Technologies, School of Physics, Sun Yat-sen University, Guangzhou 510275, China*

(Dated: June 16, 2022)

Weak superconducting proximity effect in the vicinity of the topological transition of a quantum anomalous Hall system has been proposed as a venue to realize a topological superconducting phase with chiral Majorana edge modes. Recently, experimental evidence of such chiral Majorana modes has been observed in the form of a half-integer quantized plateau in the two-terminal transport measurement. In this work we propose a non-topological mechanism for such a conductance plateau, which might also arise from the interplay of percolation of quantum Hall edges in a disordered quantum anomalous Hall system and superconductivity. We find that a half-integer quantized plateau, similar to that expected from chiral Majorana modes, can arise in the limit of weak superconductivity compared to disorder. Our work, therefore, suggests that in order to confirm the topological superconducting nature of the phase, it is necessary to supplement the electrical conductance measurements with heat transport signatures that would ensure the presence of a spectral gap underneath the superconducting region.

Recent years have seen a burgeoning interest in realizing topological superconductors which host zero-energy Majorana modes. These Majorana zero modes are not only of fundamental interest but also hold potential applications for a fault-tolerant topological quantum computation [1] owing to their non-Abelian braiding statistics [2, 3]. The Majorana modes can be found in the vortex cores of a two-dimensional (2D) chiral topological superconductors (TSCs) with an odd integer Chern number. Recent theoretical studies [4–6] proposed to realize this chiral TSC using a quantum anomalous Hall insulator (QAHI) in proximity to an *s*-wave superconductor (SC).

The quantum anomalous Hall (QAH) state is a quantum Hall (QH) state without an external magnetic field which can be realized in a 2D thin film of magnetic topological insulator (TI) with ferromagnetic ordering [7–11]. For the regime where the ferromagnetic-induced exchange field strength  $|\lambda|$  is greater than the hybridization gap  $|m_0|$  induced by the coupling between the top and bottom surfaces, the system has a Chern number  $\mathcal{C} = \lambda/|\lambda|$  and in the opposite limit where  $|\lambda| < |m_0|$ ,  $\mathcal{C} = 0$  [6, 12]. By changing the applied magnetic field over a relatively small range, a topological phase transition can be induced between the QAHI with  $\mathcal{C} = 1$  and the trivial insulator state with  $\mathcal{C} = 0$ . When the QAH is proximitized by an *s*-wave SC, the  $\mathcal{C} = 1$  and  $\mathcal{C} = 0$  phases are driven into  $\mathcal{N} = 2$  and  $\mathcal{N} = 0$  TSC, respectively. At the transition between these two phases, there exists an  $\mathcal{N} = 1$  TSC [4, 5]. This TSC has a full pairing bulk gap and  $\mathcal{N} = 1$  gapless chiral Majorana edge mode (CMEM) at the edge. Since the CMEM carries one-half of the incoming charges, it manifests as a half-integer quantized plateau  $e^2/2h$  in the conductance

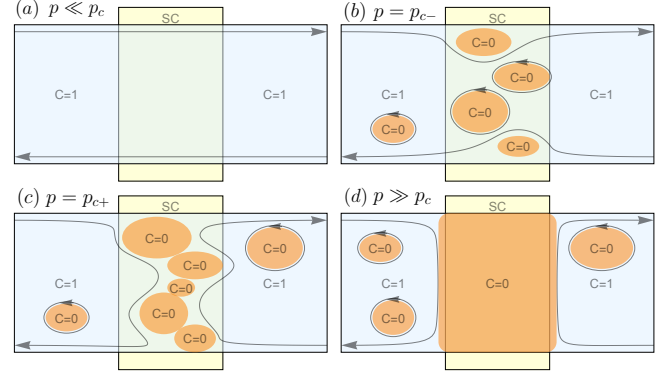


FIG. 1. (Color online) Schematics of the magnetic-field induced percolation in a disordered QAHI-SC-QAHI junction. The middle QAHI region is proximitized by an *s*-wave SC (yellow rectangle). Four different percolation stages of trivial insulator phases with  $\mathcal{C} = 0$  (orange region) in the QAHI phase with  $\mathcal{C} = 1$  (light-blue region). These four stages are characterized by different values of  $p$ , the proportion of  $\mathcal{C} = 0$  phase, which changes with magnetic field. (a) In the strong magnetic field regime where  $p$  is far below the percolation threshold ( $p \ll p_c$ ), the system is in the  $\mathcal{C} = 1$  phase. The edge states (shown by arrowed lines) are perfectly transmitted across the junction. (b) During the magnetization reversal, the  $\mathcal{C} = 0$  phase domains grow. The edge states wind around the domains in the superconducting region. (c) When  $p$  is slightly above the percolation threshold ( $p = p_{c+}$ ), the domains are connected across the width of the junction and the edge states can no longer be transmitted across the junction. (d) When  $p \gg p_c$ , the edge states are normally reflected by the  $\mathcal{C} = 0$  phase in the SC region.

measured between two normal leads and an integer quantized  $e^2/h$  peak in the conductance between a normal lead and the SC during the magnetization reversal. Re-

cent experiment [13] observed these two transport signatures in a doped magnetic QAHI thin film proximitized by an  $s$ -wave SC [5, 6]. While these transport signatures are consistent with the existence of  $\mathcal{N} = 1$  TSC with a single CMEM for a clean system, the experimental system, however, is strongly disordered with a lot of subgap states which destabilize the  $\mathcal{N} = 1$  TSC state.

In this Letter, we show that these two transport signatures can generically occur in a disordered QAHI-SC-QAHI junction even in the absence of CMEMs. Here, the SC region is the QAHI placed in proximity to an  $s$ -wave superconductor. We consider the system to be inhomogeneous but with smoothly varying magnetization [14]. It was argued in Ref. [15] that these inhomogeneity-induced domain walls are required to understand the transport properties in the QAHI-SC-QAHI system such as the Hall conductance. Figure 1 shows the evolution of the phases in the QAH state as the magnetic field is varied. In the limit of strong magnetic field, the system is in a single-domain  $\mathcal{C} = 1$  phase [as shown in Fig. 1(a)] with large average magnetization. In this regime, the edge states are perfectly transmitted across the junction. During the magnetization reversal, the proportion  $p$  of the  $\mathcal{C} = 0$  domain increases where the average magnetization in the  $\mathcal{C} = 0$  domain is small. At the boundary between the  $\mathcal{C} = 0$  and  $\mathcal{C} = 1$  domains, there exists a chiral edge state. As a result, the electron trajectory  $L$  inside the superconducting region increases as the electron has to wind around the domain which in turn increases and decreases the Andreev and normal scattering probabilities, respectively. Since  $L \rightarrow \infty$  as  $p \rightarrow p_c$  and due to the particle-hole symmetry, the electron at zero energy undergoes equal amount of normal and Andreev scattering processes which results in an  $e^2/2h$  two-terminal conductance plateau. When  $p = p_c$ , the electron can no longer be transmitted across the junction as the  $\mathcal{C} = 0$  domains become connected into a cluster spanning across the width of the junction. As  $p$  increases from  $p_c$ ,  $L$  becomes shorter which in turn increases and decreases the normal and Andreev scattering probabilities, respectively. For  $p \gg p_c$ , the system is in the  $\mathcal{C} = 0$  phase and electrons undergo perfect normal reflections outside the superconducting region as shown in Fig. 1(d). In what follows we perform a more quantitative analysis of the above picture to yield consistency with experiment.

We describe the low-energy edge modes of the QAHI-SC structure by a one-dimensional Hamiltonian:

$$H(x) = \frac{1}{2} \int dx \mathcal{C}^\dagger(x) \mathcal{H}_{\text{BdG}}(x) \mathcal{C}(x), \quad (1)$$

where

$$\mathcal{H}_{\text{BdG}}(x) = -iv\tau_0\partial_x - \mu(x)\tau_z + \frac{1}{2} \{-i\partial_x, \Delta(x)\tau_x\} \quad (2)$$

is the Bogoliubov-de Gennes (BdG) Hamiltonian and  $\mathcal{C}(x) = (c(x), c^\dagger(x))^T$  is the Nambu spinor with  $c(x)$  and

$c^\dagger(x)$  being the electron annihilation and creation operators, respectively. Here,  $v$  is the edge mode velocity,  $\mu$  is the chemical potential,  $\Delta$  is the effective  $p$ -wave pairing potential of the proximity-induced superconductivity,  $\tau_{x,y,z}$  are the Pauli matrices acting on the particle-hole space. For simplicity, we work in the units where the Planck constant  $\hbar$ , Boltzmann constant  $k_B$  and edge velocity  $v$  are set to 1. We note that the term  $\partial_x$  in the Hamiltonian comes with the anticommutation relation  $\{\cdot, \cdot\}$  to ensure the Hermiticity of the Hamiltonian. The  $p$ -wave pairing amplitude  $\Delta(x)$  is induced from the proximity effect of an  $s$ -wave superconductor with amplitude  $\Delta_0(x)$ . This cannot occur in a strictly spin-polarized edge state. However, since the QAH system arises from a TI, which is a strongly spin-orbit-coupled system, we expect the spin-polarization of the chiral edge state to vary with  $k$  (similar to the spin-texture in a TI [16] on a scale  $k_{\text{so}}$  which is related to the exchange field  $\lambda$  (i.e.,  $k_{\text{so}} \sim \lambda/v$ ). Within this model we would estimate  $\Delta(x) \sim v\Delta_0(x)/\lambda$ .

We consider a QAHI-SC-QAHI junction (as shown in Fig. 1) with spatially varying  $\mu(x)$  and  $\Delta(x)$  which naturally occurs in typical QAH systems due to the presence of magnetic dopants. For the QAHI region, we set  $\mu = \Delta = 0$ , while for the SC region, we set  $\mu(x)$  and  $\Delta(x)$  to be spatially varying along the electron trajectory length  $L$  (see Supplemental Material [17] for the spatial profile).

We can write down the scattering matrix at energy  $E$  which relates the incoming and outgoing modes at the QAHI-SC boundaries as

$$\mathcal{S}(E) = \begin{pmatrix} s_N(E) & s_A^*(-E) \\ s_A(E) & s_N^*(-E) \end{pmatrix}, \quad (3)$$

where

$$\mathcal{S} = \begin{cases} \mathcal{T}, & \text{for } p < p_c, \\ \mathcal{R}, & \text{for } p > p_c, \end{cases} \quad (4)$$

with  $\mathcal{T}$  and  $\mathcal{R}$  denoting the coherence transmission and reflection, respectively. Note that the reflection and transmission matrices can be written separately as the edge states do not undergo backscattering and also do not couple to each other. As a result, they can either be transmitted (i.e.,  $\mathcal{T} = \mathcal{S}$  and  $\mathcal{R} = 0$ ) for  $p < p_c$  or reflected (i.e.,  $\mathcal{R} = \mathcal{S}$  and  $\mathcal{T} = 0$ ) for  $p > p_c$ . The scattering matrix elements can be calculated by matching the incoming and outgoing modes in the SC region (see Supplemental Material [17] for the derivation), which yields

$$\mathcal{S}(E) = \prod_j e^{i\tilde{v}_j^{-1/2}(\mu_j\tau_z + E\tau_0)\tilde{v}_j^{-1/2}\ell}, \quad (5)$$

where  $\tilde{v}_j = v\tau_0 + \Delta_j\tau_x$  is the effective edge mode velocity along region  $j$  with chemical potential  $\mu_j$  and pairing potential  $\Delta_j$ . Since the scattering matrix in the QAHI region gives just a phase factor in the current amplitude,

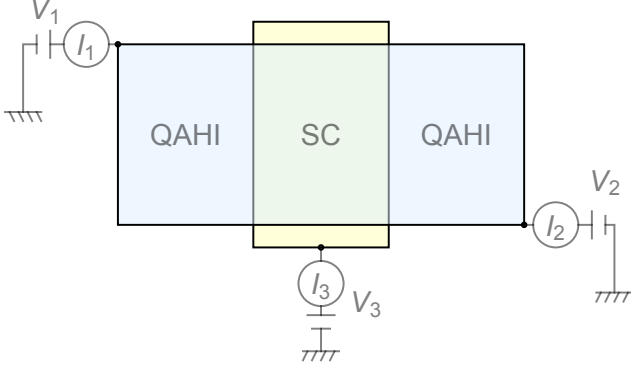


FIG. 2. (Color online) Schematic diagram of the setup used to measure the conductance in a QAHI-SC-QAHI junction. For the case where  $G_{12}$  is measured, we consider the SC to be floating (i.e., the current  $I_3 = 0$ ) and the voltages  $V_1$  and  $V_2$  to be applied to leads 1 and 2, respectively. For the case where  $G_{13}$  is measured, the SC is grounded (i.e.,  $I_3 \neq 0$ ), lead 2 is removed, the voltages  $V_1$  and  $V_3$  are applied to leads 1 and SC, respectively.

the length of QAHI region does not change the conductance and hence can be ignored in the calculation.

We study the conductance within the linear response where the voltage is near zero energy. The conductance of the junction is related to the difference between the zero-temperature normal and Andreev scattering probabilities  $\delta S_0(E) = |s_N(E)|^2 - |s_A(E)|^2$ . At finite temperature  $T$ ,  $\delta S$  at zero energy can be computed from the zero-temperature  $\delta S_0(E)$  by a convolution with the derivative of Fermi distribution, i.e.,

$$\delta S = \int dE \left( -\frac{\partial f_T(E)}{\partial E} \right) (|s_N(E)|^2 - |s_A(E)|^2), \quad (6)$$

where  $f_T(E) = 1/(e^{(E-\mu_{\text{QAHI}})/T} + 1)$  is the Fermi distribution with  $\mu_{\text{QAHI}} = 0$  being the chemical potential of the QAHI.

The conductance is measured using the setup shown in Fig. 2. Within the generalized Landauer-Büttiker transport formalism for a normal-superconductor interface [18, 19], the current flowing in leads 1 and 2 are given by

$$I_1 = \frac{e^2}{h} [(1 - \delta\mathcal{R})(V_1 - V_3) - \delta\mathcal{T}(V_2 - V_3)], \quad (7a)$$

$$I_2 = \frac{e^2}{h} [-\delta\mathcal{T}'(V_1 - V_3) + (1 - \delta\mathcal{R}')(V_2 - V_3)], \quad (7b)$$

where  $V_1$  and  $V_2$  are the voltages applied to leads 1 and 2, respectively, and  $V_3$  is the voltage of the SC which is set to 0. Here,  $\delta\mathcal{R}$  and  $\delta\mathcal{T}$  are the net reflection and transmission probabilities for the left-incoming electron, respectively while  $\delta\mathcal{R}'$  and  $\delta\mathcal{T}'$  are the net reflection and transmission probabilities for the right-incoming electron, respectively.

We consider two kinds of measurement setups: floating and grounding SC. For the case of floating SC, there is no current flowing from the SC to the ground ( $I_3 = 0$ ). Using Eq. (7) and the current conservation equation ( $I_1 + I_2 = 0$ ), we obtain the conductance between leads 1 and 2 as

$$G_{12} \equiv \frac{I_1}{V_1 - V_2} = \frac{e^2}{h} \left[ \frac{\delta\mathcal{T}\delta\mathcal{T}' - (1 - \delta\mathcal{R})(1 - \delta\mathcal{R}')}{\delta\mathcal{T} + \delta\mathcal{T}' + \delta\mathcal{R} + \delta\mathcal{R}' - 2} \right]. \quad (8)$$

For the second case where the SC is grounded, there is a current flowing from the SC to the ground ( $I_3 \neq 0$ ). For this scheme, we consider removing lead 2 ( $I_2 = 0$ ). Applying Eq. (7) for this case, we obtain the conductance between lead 1 and SC as

$$G_{13} \equiv \frac{I_1}{V_1 - V_3} = \frac{e^2}{h} \left[ \frac{(1 - \delta\mathcal{R})(1 - \delta\mathcal{R}') - \delta\mathcal{T}\delta\mathcal{T}'}{1 - \delta\mathcal{R}'} \right]. \quad (9)$$

To understand how the percolation picture shown in Fig. 1 gives rise to a half-integer quantized conductance plateau in  $G_{12}$  and an integer quantized conductance peak in  $G_{13}$ , let us first look at the difference between the disorder-averaged zero-energy normal and Andreev scattering probabilities  $\overline{\delta S}$  (calculated using Eq. (6)) as a function of the electron trajectory length  $L/\bar{\eta}$  as plotted in Fig. 3 where  $\bar{\eta} = vk_{\text{so}}/\Delta_0(x)$  is the disorder-averaged dimensionless superconducting coherence length. Note that the superconducting coherence length is dimensionless because of the  $p$ -wave pairing, which makes it essential to introduce the scale  $k_{\text{so}} \sim (50 \text{ nm})^{-1}$ . From Fig. 3, we can see that  $\overline{\delta S}$  decays exponentially with  $L$ . This exponential decay can be understood by first rewriting the scattering matrix  $\bar{S}$  in the Majorana basis. In this basis,  $\bar{S}$  is the average of product of random SO(2) matrices which can be mapped into random walks on a circle. As a result, the quantity  $|s_N|^2 - |s_A|^2 = \cos^2 \theta - \sin^2 \theta \sim \exp(-2L\sigma^2/\ell)$  where  $\sigma$  is the standard deviation of the angle  $\theta$  that parametrizes the SO(2) matrix (see Supplementary material [20] for a proof).

The length of the electron trajectory  $L$ , which is the outer perimeter of a cluster comprising the connected  $\mathcal{C} = 0$  domains, increases as the proportion  $p \rightarrow p_c$  where the percolation threshold  $p_c$  corresponds to the magnetic field near the coercive field. Near  $p_c$ ,  $L$  obeys the scaling relation [21]:

$$L = L_0 |p - p_c|^{-(1+\nu)d_f}. \quad (10)$$

Here, the correlation length exponent  $\nu$  is  $\frac{4}{3}$  [22], the fractal dimension of the cluster  $d_f$  is  $\frac{91}{48}$  [23] for two dimensions. For the numerical simulation done in this paper, we choose  $L_0$  to be  $500\bar{\eta}$  so that the conductance plateau width is in a small region near the percolation threshold  $p_c$ . Since  $L \rightarrow \infty$  as  $p \rightarrow p_c$ ,  $\overline{\delta S} \rightarrow 0$  as  $p \rightarrow p_c$ . This fact together with the particle-hole symmetry means that at  $p = p_c$ , there are equal normal and Andreev scattering

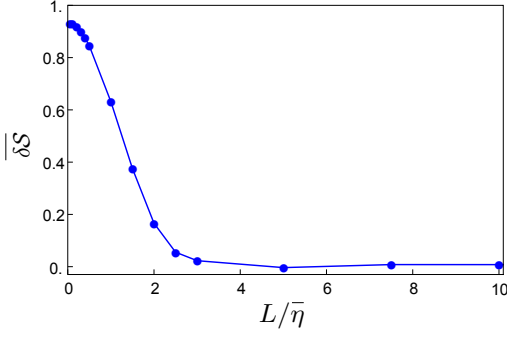


FIG. 3. (Color online) Disorder-averaged zero-energy net scattering probability ( $\overline{\delta S} = |s_N|^2 - |s_A|^2$ ), which is the difference between the normal and Andreev scattering probabilities, as a function of electron trajectory length  $L/\bar{\eta}$  where  $\bar{\eta} = v/\Delta$  is a dimensionless disorder-averaged superconducting coherence length. Note that  $\overline{\delta S}$  exponentially decays with  $L$ . For  $p < p_c$ , there is only coherence transmission process ( $\delta S = \delta T$  and  $\delta R = 0$ ), while for  $p > p_c$ , there is only coherence reflection process ( $\delta S = \delta R$  and  $\delta T = 0$ ). We consider the disorder in  $\Delta$  and  $\mu$  where the values of  $\Delta \in [0, 0.1]$  and  $\mu \in [-0.01, 0.01]$  are drawn from uniform distributions. Parameters used are edge mode velocity  $v = 1$  and temperature  $T = 0.3$ .

probabilities at zero energy, giving rise to a half-integer quantized conductance in  $G_{12}$  and an integer quantized conductance in  $G_{13}$ .

From the value of  $\overline{\delta S}$ , we calculate the conductances  $G_{12}$  and  $G_{13}$  using Eqs. (8) and (9). Figure 4 shows the disorder-averaged  $\overline{G}_{12}$  and  $\overline{G}_{13}$  as a function of  $p - p_c$  near the percolation threshold  $p_c$ . As can be seen from the plot, the conductance  $\overline{G}_{12} \simeq e^2/h$  for  $p < p_c$  and  $\overline{G}_{12} \simeq 0$  for  $p > p_c$  with a plateau at  $e^2/2h$  near  $p_c$  while the conductance  $\overline{G}_{13} \simeq 0$  for  $p < p_c$  and  $p > p_c$  with a peak at  $e^2/h$  near  $p_c$ . The conductance plateau of  $\overline{G}_{12}$  and peak of  $\overline{G}_{13}$  near  $p_c$  are due to the fact that  $\overline{\delta S}$  decays exponentially with  $L$  as  $p \rightarrow p_c$ . We note that these two signatures, which originate from the disorder effect, resemble the experimental data [13] claimed to be the signatures of CMEMs.

Our simplified model relies on a classical percolation model for the QH transition where the chiral edge effectively becomes long enough to produce the plateaus in Fig. 4. This classical percolation picture may be considered as a reasonable description of the QH transition only up to some finite distance from the critical point or at a relatively high temperature. Arbitrarily close to the critical point and at low temperatures, it is necessary to switch to a more quantum mechanical description such as quantum percolation [14, 24]. This limitation is justified at the relatively high temperatures of the experiment that prevent access to the QH transition in any case. Finite temperature is also crucial for allowing us to consider a disorder averaging for the transmission prob-

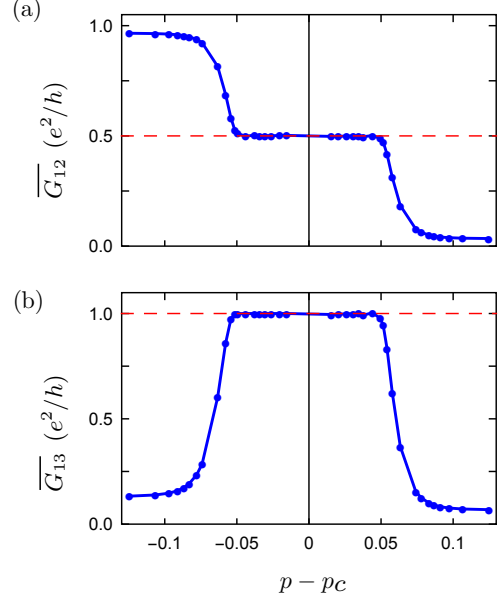


FIG. 4. (Color online) Disorder-averaged conductance (a)  $\overline{G}_{12}$  and (b)  $\overline{G}_{13}$  as a function of  $p$  near the percolation threshold  $p_c$ . The parameters used here are the same as those used in Fig. 3.  $\overline{G}_{12}$  exhibits a half-integer quantized plateau near  $p_c$  while  $\overline{G}_{13}$  shows an integer quantized peak near  $p_c$ .

abilities. Technically, a single system with elastic impurity scatterings is a fixed disorder realization and would lead to strong mesoscopic fluctuations in the transmission probability. Thermal noise leads to time-dependent fluctuations of the disorder potential that are averaged over justifying the averaging. The inclusion of a finite electron temperature also plays a role in the suppression of such mesoscopic fluctuations.

Despite the simplified classical nature of our analysis, we do expect our results to remain valid for related reasons even at the lowest temperature. To understand this, we discuss some general expectations based on field theory for the system. Based on the argument in the introduction, the system must cross through the  $\mathcal{N} = 1$  TSC phase as the magnetization is changed in the clean system limit. Furthermore, this phase and its associated phase transition are stable to weak disorder [25]. However, given the experimental QAH system is a highly doped TI with weak proximity effect, it is more appropriate to consider the phase arising in the vicinity of the QH transition in the limit of strong disorder with the superconductivity being considered as a perturbation. The regular QH transition is described by localized states and a quantized Hall quantity at the Fermi level except at a critical point where the localization length diverges. The phase in this region is essentially described by a metallic phase with finite longitudinal conductivity. In the absence of superconductivity, this metallic phase occurs at a critical point in the parameter space and is not a

plateau unlike Fig. 4. However, the addition of superconductivity creates the possibility of a different phase that arises from the hybridization of the SC gap with the nearly delocalized states near the transition. The nearly delocalized normal states together with SC likely forms a delocalized states with SC – referred to as the thermal metal [25]. This phase has been shown to be stable against Anderson localization and to develop a divergent density of states of conducting states at the Fermi level [25]. Such a thermal metallic state destabilizes the chiral edge states underneath the SC region. Assuming that the SC region perturbs the system sufficiently such that the region outside the SC remains deep in the QAH phase, one expects the chiral edge state in the QAH region to essentially disappear into the metallic phase underneath the SC. This leads to a vanishing net transmission and reflection between the incoming and outgoing chiral edges from the SC ( $\delta\mathcal{T}, \delta\mathcal{R} \rightarrow 0$ ), which are the necessary and sufficient conditions giving rise to the  $e^2/2h$  conductance (according to Eq. (8)).

Using the percolation picture, we have shown that the half-integer quantized conductance plateau in  $G_{12}$  and integer quantized conductance peak in  $G_{13}$  can arise generically in a disordered QAHI-SC-QAHI junction. While the TSC phase is inevitable in the vicinity of the QH transition in a weakly disordered system, strongly disordered systems can lead to a much more complicated conventional Chern insulator phase with a larger density of states either from a long edge (classical percolation) or the thermal metal phase. Unfortunately, as evident from Fig. 4 of our results, the classical percolation phase as well as the low-temperature thermal metal phase would lead to the  $e^2/2h$  signature observed in this system. A smoking-gun test to avoid this would be to measure the associated thermal Hall conductivity of the system. Alternatively, and more simply, a measurement of the thermal conductance or heat capacity would reveal if the system underneath the SC is truly in a gapped phase in the putative topological region as opposed to the gapless phase considered in this manuscript. Both the classical percolation-based model as well as the thermal metal phase would have large longitudinal thermal conductance and make the thermal Hall conductance non-universal.

We thank K. T. Law for valuable discussions that drew our attention to Ref. [13] which motivated this work. J.S. acknowledges stimulating discussion with S.-C. Zhang that motivated the discussion of the low-temperature limit. We also thank Yahya Alavirad, Ching-Kai Chiu and Qing Lin He for helpful discussions. This work is supported by JQI-NSF-PFC. Y.H. is grateful to China Scholarship Council for financial support. J.D.S. acknowledges the funding from Sloan Research Fellowship and NSF-DMR-1555135 (CAREER). We acknowledge the University of Maryland supercomputing resources

(<http://www.it.umd.edu/hpcc>) made available in conducting the research reported in this paper.

*Note added* During the final stages of writing the draft, we became aware of a recent manuscript [26] related to our work.

- 
- [1] C. Nayak, S. H. Simon, A. Stern, M. Freedman, and S. Das Sarma, *Rev. Mod. Phys.* **80**, 1083 (2008).
  - [2] N. Read and D. Green, *Phys. Rev. B* **61**, 10267 (2000).
  - [3] D. A. Ivanov, *Phys. Rev. Lett.* **86**, 268 (2001).
  - [4] X.-L. Qi, T. L. Hughes, and S.-C. Zhang, *Phys. Rev. B* **82**, 184516 (2010).
  - [5] S. B. Chung, X.-L. Qi, J. Maciejko, and S.-C. Zhang, *Phys. Rev. B* **83**, 100512 (2011).
  - [6] J. Wang, Q. Zhou, B. Lian, and S.-C. Zhang, *Phys. Rev. B* **92**, 064520 (2015).
  - [7] X.-L. Qi, Y.-S. Wu, and S.-C. Zhang, *Phys. Rev. B* **74**, 085308 (2006).
  - [8] C.-X. Liu, X.-L. Qi, X. Dai, Z. Fang, and S.-C. Zhang, *Phys. Rev. Lett.* **101**, 146802 (2008).
  - [9] C.-X. Liu, S.-C. Zhang, and X.-L. Qi, *Annu. Rev. Condens. Matter Phys.* **7** (2016).
  - [10] R. Yu, W. Zhang, H.-J. Zhang, S.-C. Zhang, X. Dai, and Z. Fang, *Science* **329**, 61 (2010).
  - [11] C.-Z. Chang, J. Zhang, X. Feng, J. Shen, Z. Zhang, M. Guo, K. Li, Y. Ou, P. Wei, L.-L. Wang, *et al.*, *Science* **340**, 167 (2013).
  - [12] J. Wang, B. Lian, and S.-C. Zhang, *Phys. Rev. B* **89**, 085106 (2014).
  - [13] Q. L. He, L. Pan, A. L. Stern, E. C. Burks, X. Che, G. Yin, J. Wang, B. Lian, Q. Zhou, E. S. Choi, K. Murata, X. Kou, Z. Chen, T. Nie, Q. Shao, Y. Fan, S.-C. Zhang, K. Liu, J. Xia, and K. L. Wang, *Science* **357**, 294 (2017).
  - [14] J. Chalker and P. Coddington, *Journal of Physics C: Solid State Physics* **21**, 2665 (1988).
  - [15] C.-Z. Chen, J. J. He, D.-H. Xu, and K. T. Law, *Phys. Rev. B* **96**, 041118 (2017).
  - [16] M. Z. Hasan and C. L. Kane, *Rev. Mod. Phys.* **82**, 3045 (2010).
  - [17] See Sec. I of the Supplemental Material for detailed derivations of the scattering matrix.
  - [18] M. P. Anantram and S. Datta, *Phys. Rev. B* **53**, 16390 (1996).
  - [19] O. Entin-Wohlman, Y. Imry, and A. Aharony, *Phys. Rev. B* **78**, 224510 (2008).
  - [20] See Sec. II of the Supplemental Material for a proof of the exponential decay of  $\delta\mathcal{S}$  with  $L$ .
  - [21] M. B. Isichenko, *Rev. Mod. Phys.* **64**, 961 (1992).
  - [22] B. Nienhuis, *Phys. Rev. Lett.* **49**, 1062 (1982).
  - [23] A. Kapitulnik, A. Aharony, G. Deutscher, and D. Stauffer, *Journal of Physics A: Mathematical and General* **16**, L269 (1983).
  - [24] B. Huckestein, *Rev. Mod. Phys.* **67**, 357 (1995).
  - [25] T. Senthil and M. P. A. Fisher, *Phys. Rev. B* **61**, 9690 (2000).
  - [26] W. Ji and X.-G. Wen, *arXiv:1708.06214* (2017).

## Supplemental Material

### I. SCATTERING MATRIX

Using the BdG Hamiltonian in Eq. (2), we can write the Schrödinger equation  $\mathcal{H}_{\text{BdG}}\psi = E\psi$  for the edge state as

$$-i\tilde{v}(x)\partial_x\psi_E(x) = \left(E\tau_0 + \mu(x)\tau_z + \frac{1}{2}i\partial_x\tilde{v}(x)\right)\psi_E(x), \quad (\text{S-1})$$

where  $\tilde{v}(x) = v\tau_0 + \Delta(x)\tau_x$  is the effective edge mode velocity. As shown in Fig. S1, we assume  $\tilde{v}(x)$  to be spatially varying along the electron trajectory  $L$  in the SC region where  $\tilde{v}(x)$  jumps at the boundaries (at  $x = x_0, \dots, x_N$ ). Since  $\partial_x\tilde{v}(x) \gg E, \mu$  at the boundaries, integrating Eq. (S-1) at the boundaries yields

$$\psi_E(x_{j+}) = \frac{\tilde{v}_j^{1/2}}{\tilde{v}_{j+1}^{1/2}}\psi_E(x_{j-}). \quad (\text{S-2})$$

Here,  $x_{j\pm}$  is the position just to the right/left of the boundary  $j$ . In the region between  $x_{j-1}$  and  $x_j$ ,  $\tilde{v}(x) = \text{const}$ , so we have

$$\psi_E(x_{j-}) = e^{i\tilde{v}_j^{-1}(\mu_j\tau_z + E\tau_0)\ell}\psi_E(x_{(j-1)+}). \quad (\text{S-3})$$

Using the Baker-Campbell-Hausdorff formula  $e^{iA^{-1}B} = A^{-1/2}e^{iA^{-1/2}BA^{-1/2}}A^{1/2}$ , we can write down Eq. (S-3) as

$$\psi_E(x_{j-}) = \tilde{v}_j^{-1/2}e^{i\tilde{v}_j^{-1/2}(\mu_j\tau_z + E\tau_0)\tilde{v}_j^{-1/2}\ell}\tilde{v}_j^{1/2}\psi_E(x_{(j-1)+}). \quad (\text{S-4})$$

The outgoing current amplitude at  $x_N = L$  is then given by

$$\mathcal{J}_{\text{out}}(E) = \prod_j^N e^{i\tilde{v}_j^{-1/2}(\mu_j\tau_z + E\tau_0)\tilde{v}_j^{-1/2}\ell}\mathcal{J}_{\text{in}}(E), \quad (\text{S-5})$$

where  $\mathcal{J}_{\text{out}}(E) = \sqrt{v}\psi_E(x_N)$  and  $\mathcal{J}_{\text{in}}(E) = \sqrt{v}\psi_E(x_0)$  are the outgoing and incoming current amplitudes in the SC region. The scattering matrix is given by

$$\mathcal{S}(E) = \prod_j^N e^{i\tilde{v}_j^{-1/2}(\mu_j\tau_z + E\tau_0)\tilde{v}_j^{-1/2}\ell}. \quad (\text{S-6})$$

### II. PROOF FOR EXPONENTIAL DECAY OF $\overline{\delta S}$ WITH $L$

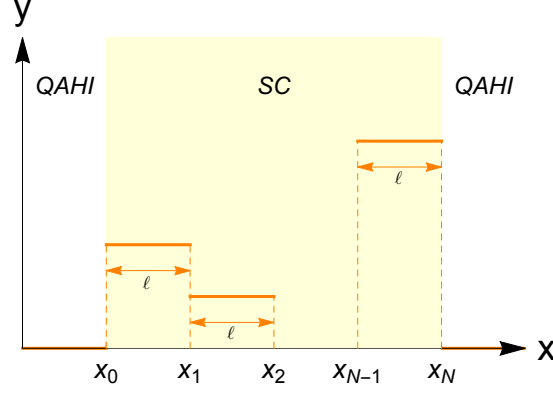
In the Majorana basis  $\tilde{\mathcal{C}}_j \equiv \Lambda\mathcal{C}_j = \frac{1}{\sqrt{2}}(c_j + c_j^\dagger, ic_j - ic_j^\dagger)^T$  where  $\Lambda = \frac{1}{\sqrt{2}}\begin{pmatrix} 1 & 1 \\ i & -i \end{pmatrix}$ , the scattering matrix is given by  $\tilde{\mathcal{S}} \equiv \Lambda\mathcal{S}\Lambda^\dagger$ . Using the Baker-Campbell-Hausdorff formula  $\Lambda e^A \Lambda^\dagger = e^{\Lambda A \Lambda^\dagger}$  and  $\Lambda(\prod_j \mathcal{S}_j)\Lambda^\dagger = \prod_j (\Lambda\mathcal{S}_j\Lambda^\dagger)$  for unitary matrix  $\Lambda$ , we can write the scattering matrix as  $\tilde{\mathcal{S}} \equiv \prod_j \tilde{\mathcal{S}}_j$ . The zero-energy scattering matrix is then given by

$$\tilde{\mathcal{S}} = \prod_j \begin{pmatrix} \cos\theta_j & \sin\theta_j \\ -\sin\theta_j & \cos\theta_j \end{pmatrix} \quad (\text{S-7})$$

with  $\theta_j = \frac{\mu\ell}{v\sqrt{1-\Delta_j^2}}$  where  $N = L/\ell$ .

Since  $\tilde{\mathcal{S}}_j$  is real and unitary, it is in the  $\text{SO}(2)$  group. The  $\text{SO}(2)$  group has the following relation

$$\prod_j \tilde{\mathcal{S}}_j(\theta_j) = \tilde{\mathcal{S}}(\sum_j \theta_j), \quad (\text{S-8})$$



Supplementary Figure S1. (Color online) Spatial variation of  $\mu, \Delta$  along the electron trajectory  $L$ . The length over which  $\Delta$  and  $\mu$  remains constant is  $\ell$ . For the numerical simulation done in this paper, we set  $\ell = 0.05\bar{\eta}$ .

where  $\theta_j \in [-\pi, \pi]$ . If  $\theta_1, \theta_2, \theta_3, \dots, \theta_N$  are independent and identically distributed random variables, each with mean  $\bar{\theta}$  and variance  $\sigma^2$ , for sufficiently large  $N$  the sum of the angle  $\Theta = \sum_j \theta_j$ , according to the central limit theorem, has a normal distribution  $f(\Theta) = \frac{1}{\sqrt{2\pi N\sigma^2}} e^{-\frac{(\Theta - N\bar{\theta})^2}{2N\sigma^2}}$  with mean  $\bar{\Theta} = N\bar{\theta}$  and variance  $N\sigma^2$ .

The net scattering probabilities is  $\delta\tilde{\mathcal{S}} = |s_N|^2 - |s_A|^2 = \cos 2\Theta$  with its expectation value given by

$$\begin{aligned} \overline{\delta\tilde{\mathcal{S}}} &= \int_{-N\pi}^{N\pi} f(\Theta) \cos(2\Theta) \\ &\approx -\frac{1}{4} e^{-2N\sigma^2} \cos(2N\bar{\theta}) \left( \operatorname{erf}\left(\frac{\sqrt{N}(\bar{\theta} - \pi)}{\sqrt{2}\sigma}\right) - \operatorname{erf}\left(\frac{\sqrt{N}(\bar{\theta} + \pi)}{\sqrt{2}\sigma}\right) \right) \\ &\approx \frac{1}{2} e^{-2N\sigma^2} \cos(2N\bar{\theta}) - \frac{\sigma \cos(2N\bar{\theta})}{2\sqrt{2N\pi}(\bar{\theta} + \pi)} e^{-\frac{N((\bar{\theta} + \pi)^2 + 4\sigma^4)}{2\sigma^2}} - \frac{\sigma \cos(2N\bar{\theta})}{2\sqrt{2N\pi}(\pi - \bar{\theta})} e^{-\frac{N((\bar{\theta} - \pi)^2 + 4\sigma^4)}{2\sigma^2}} + \mathcal{O}(N^{-3/2} e^{-N/2\sigma^2}). \end{aligned} \quad (\text{S-9})$$

Note that in the second line of Eq. (S-9) we have used  $\sigma^2 \ll \pi$  and in the third line we only keep terms up to  $\mathcal{O}(N^{-1/2} e^{-N/2\sigma^2})$ . Since  $e^{-2N\sigma^2}$  decays slower than  $e^{-\frac{N((\bar{\theta} + \pi)^2 + 4\sigma^4)}{2\sigma^2}}$  and  $e^{-\frac{N((\bar{\theta} - \pi)^2 + 4\sigma^4)}{2\sigma^2}}$  as  $N \rightarrow \infty$ ,  $\overline{\delta\tilde{\mathcal{S}}}$  is then given by

$$\overline{\delta\tilde{\mathcal{S}}} \propto e^{-2L\sigma^2/\ell} \quad (\text{S-10})$$

So  $\overline{\delta\tilde{\mathcal{S}}}$  decays exponentially with the electron trajectory length  $L$ .